The International Journal of Advanced Manufacturing Technology (2022) 119:2127–2144
https://doi.org/10.1007/s00170-021-08279-6

ORIGINAL ARTICLE

# Tribology and machinability performance of hybrid $Al_2O_3$ -MWCNTs nanofluids-assisted MQL for milling Ti-6Al-4 V

**Muhammad Jamil[1] · Ning He[1] · Wei Zhao[1] · Aqib Mashood Khan[1,2] · Rashid Ali Laghari[1]**

Received: 21 May 2021 / Accepted: 23 October 2021 / Published online: 2 December 2021


## Abstract
Recent burgeoning development in nanotechnology unfolded an avenue in the manufacturing industry. Owing to the superior heat transfer potential of nano-additives, it could be interesting to improve the heat transfer and tribological capability of metal cutting fluids by mixing nanofluids in emulsions properly. To attain high heat transfer performance in cutting difficult-to-cut alloys, hybrid nanofluids-assisted minimum quantity lubrication (MQL) system is applied with the anticipation of efficient lubrication and heat transfer. Taguchi $L_{16}(4^3)$ orthogonal array is used involving nanofluids concentrations, air pressure, and cooling flow rate of alumina-multiwalled carbon nanotubes ($Al_2O_3$-MWCNTs) at constant cutting conditions in the milling of Ti-6Al-4V. The resultant cutting force ($F_R$), cutting temperature ($T$), and surface roughness (Ra) are considered key machining responses. Besides, tool wear, chip analysis, and surface topography are also analyzed under the effect of hybrid nanofluids. Findings have shown the minimum resultant force, cutting temperature, and surface roughness of 24.3 N, 148.7 °C, and 0.67 μm, respectively, at nanofluids concentrations of 0.24wt.% and 120 mL/h of flow rate at 0.6 MPa of air pressure. The microscopic analysis of the end-mill depicted minor thermal damage, chip welding, and coating peeling under hybrid nanofluids machining. Also, the chip analysis depicted the clean back chip surface and less melting of saw-tooth chip edges. The surface topography confirmed less chip adhesion and material debris. Results summary showed appropriately chosen MQL parameters improving the cooling/lubrication performance by providing oil film and enhancing the milling performance measures. The outcomes of the proposed study are useful for the manufacturing industry to enhance the process performance.

**Keywords** Cutting force · Cutting temperature · Chip analysis · Surface integrity

## Abbreviations

| | |
|---|---|
| MQL | Minimum quantity lubrication |
| $f_r$ | Flow rate (mL/h) |
| MWCNT | Multiwalled carbon nanotubes |
| $A_p$ | Air pressure (MPa) |
| $F_R$ | Resultant cutting force |
| *Conc* | Nanofluids concentration (wt.%) |
| $T$ | Cutting temperature |
| MS | Mean square |
| *Ra* | Average surface roughness |
| $q$ | Shearing heat |
| BUE | Built-up edges |
| $K_0$ | Bessel function |
| EDS | Energy-dispersive X-ray spectroscopy |
| $\alpha$ | Thermal diffusivity |
| ANOVA | Analysis of variance |
| $L$ | Un-deform chip thickness |
| S/N | Signal-to-noise ratio |
| $h$ | Heat transfer coefficient |
| 3D | Three dimensional |
| $\mu m$ | Micrometer |

✉ Ning He
drnhe@nuaa.edu.cn

Muhammad Jamil
engr.jamil@nuaa.edu.cn

Wei Zhao
nuaazw@nuaa.edu.cn

Aqib Mashood Khan
dr.aqib@nuaa.edu.cn

Rashid Ali Laghari
rashidali@nuaa.edu.cn

[1] College of Mechanical and Electrical Engineering, Nanjing University of Aeronautics and Astronautics, Nanjing 210016, China

[2] Department of Mechanical Engineering, University of Engineering and Technology Lahore, Narowal Campus, Narowal 51600, Pakistan

## 1 Introduction

Ti-6Al-4V (*α-β alloy*) has become an attractive alternative due to exceptional performance at high temperature owing to strength, resistance to corrosion, and high toughness. That is why it has enormous usage in shipbuilding, automobile, aerospace, and medical industries. Ti-6Al-4 V is hard to cut, reactive to tool material at elevated temperature, and prone to the built-up edge (BUE) formation and welding of chips during cutting, with a high coefficient of friction [1]. The thermal conductivity of Ti-6Al-4 V is also less (6.7 W/mK) and accumulates heat into the workpiece material leading to surface burning, fatigue, and thermal shock.

Surface burning leads to poor surface quality and chemical reactivity accelerating the tool wear as reported by numerous researchers [2, 3]. To cope up with the challenge, it is necessary to use low cutting conditions to achieve better surface quality, low temperature, and gradual tool wear. In the meantime, low cutting conditions reduce productivity, which is unacceptable from the industrial point of view. The application of mineral-based metal cutting fluids is very common in the industry to control heat generation and to provide adequate lubrication. However, the emerging sustainable approach to reduce consumption of cutting fluids (i.e., 785 billion tons in 2018) [4], 15 ~ 17% of the coolant cost, and associated disposal cost have put forward to adopt dry or near-to-dry sustainable cooling techniques in machining.

Near-to-dry minimum quantity lubrication (MQL) is used to improve the machining characteristics during the process of medium-hard materials [5]. MQL reduced 40 ~ 60% of the lubrication cost and fluid quantity and pressurized fine coolant spray to penetrate the cutting zone effectively [6]. However, MQL effectiveness decreases significantly during machining of Ti-6Al-4 V due to high heat generation during cutting. Due to the poor thermal conductivity, this heat accumulates at the primary cutting zone enabling ease in reactivity towards cutting tool material, chip welding, and BUE formation that accelerates tool wear. The nickel-based superalloy was machined under MQL-based CNC milling through uncoated carbide tools. A comparison between mineral- and vegetable oil-assisted MQL was applied at the varying flow rate, nozzle distance, nozzle type, and type of cutting process. The performance measures were tool life and cutting forces. The findings have indicated that vegetable oil provided extended tool life at a flow rate of 100 mL/h in the up-milling process [6]. In a nutshell, MQL has the potential to limit heat generation and improving production quality and material removal rate. Considering the importance of improving the material removal rate in the industry, the addition of nanoparticles of 1–100 nm size particles dispersed in vegetable oil-based MQL has been adopted widely to improve the lubrication and thermal conductivity of a nanofluid [7]. Numerous types of nanoparticles are available in the market for various applications such as iron oxide ($Fe_2O_3$), aluminum nitride (AlN), zinc oxide (ZnO), alumina ($Al_2O_3$) [8], and single- and multiwalled carbon nanotubes (MWCNTs). The addition of a tiny volume of nano-additives in base oil significantly increases the surface area of the cooling medium, heat transfer, and stable Brownian motion of particles [9, 10]. The effect of MWCNTs-assisted MQL in the machining of Ti-6Al-4 V is investigated at varying cutting conditions. A significant decrease in surface roughness was observed due to the formation of stable tribological thin film and filled micropores on newly generated machined surface and the tool cutting edge [11]. Another study has considered the comprehensive comparison of silver and alumina nanoparticles-assisted MQL in the machining of nickel alloy. The comparison has provided exciting results about the turning performance measures. The alumina-based nanoparticles have provided less cutting force, wear, and chip curling due to the small contact angle, fine droplet, and spreadability of particles. Besides, the exceptional ball-bearing effect of silver nanofluids provided good surface quality [12] and limited abrasive wear [13]. Figure 1 depicts the key advantages of applying hybrid nanofluids [14], such as preventing the direct contact of the tool surface with the workpiece surface, filling the workpiece surface gaps, and transferring the heat from the workpiece to cutting fluids [15].

The application of hybrid nanoparticles-based MQL has been reported more effective to provide better cooling/lubrication due to the synergistic effect of both particles. Ahammed et al. mixed $Al_2O_3$-graphene nanofluids and reported an 88.62% increase in thermal conductivity and a 4.7% reduction in temperature in mini-channel heat exchangers [16]. An attempt has been made to investigate the $Al_2O_3$-MWCNTs hybrid nanofluids to evaluate the effect of temperature, surface roughness, and tool life in the machining of hard materials. The hybrid nanoparticles were dispersed in vegetable oil. Results have shown that hybrid nanofluids have improved surface finish by 8.72%, cutting force by 11.8%, and tool life by 23% compared to cryogenic-$CO_2$ cooling [17]. Similarly, Nine et al. have combined $Al_2O_3$-MWCNTs and reported an improvement in thermal conductivity [18]. Zhang et al. have applied $MoS_2$-MWCNTs in the grinding process and reported lower grinding ratio and surface roughness than individual mixed $MoS_2$ or MWCNTs nano-additives [19]. Furthermore, MWCNTs nano-additives-based MQL has been applied in the machining of titanium dispersed in vegetable oil in different concentrations to optimize the turning process. Results have concluded that 2

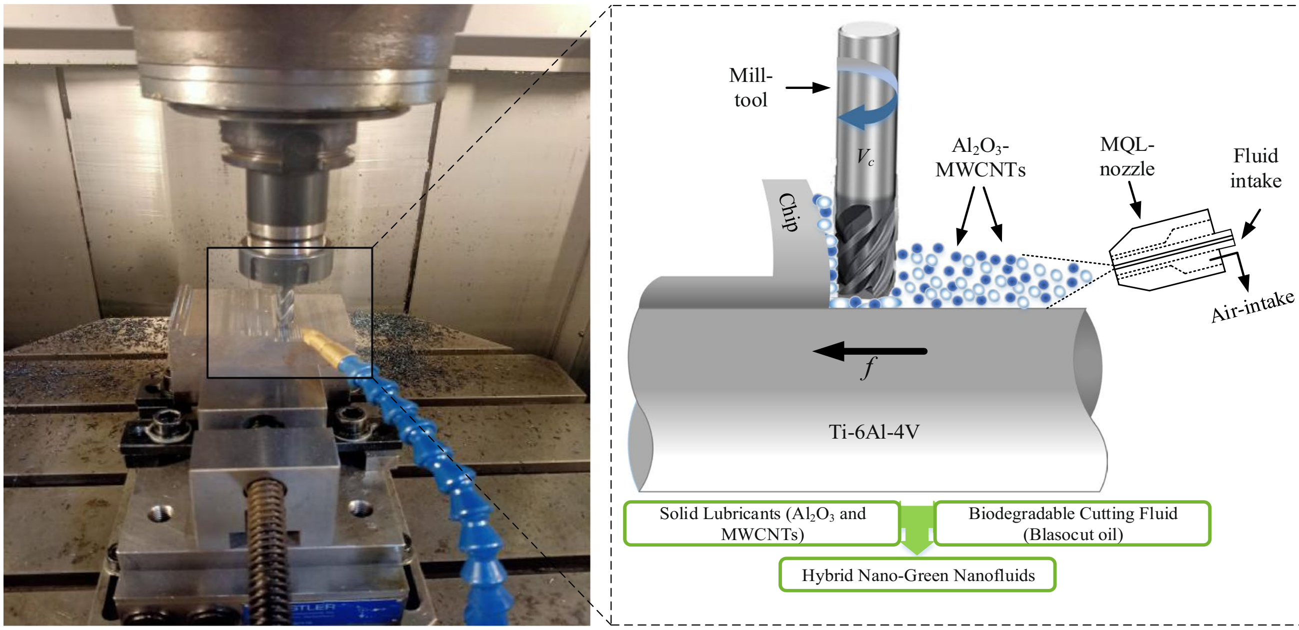


**Fig. 1** Application of hybrid nanofluids through the minimum quantity lubrication system

wt% MWCNTs reduced power by 11.5% compared to MQL without additives [20].

To improve the thermal and tribological characteristics of nanofluids, $Al_2O_3$-MWCNTs have been applied in different concentrations. The study showed a significant reduction in wear and friction coefficient due to excellent lubrication, wettability, and dispersion. Besides, hybrid nanofluids have reduced flank wear by 11% and nodal temperature by 27.36% as compared to only $Al_2O_3$-based MQL cooling/lubrication [21]. The spherical shape $Al_2O_3$ nano-additives and cylindrical morphology of MWCNTs have different sizes that can penetrate in depth. In addition, MWCNTs have weak van der Waal forces and easily shear under external load. A significant reduction of friction coefficient can also be associated with inter-tubular slip at the tool-chip interface. Thermal conductivity of MWCNTs is very high (3000 ~ 6000 W/m°C) that dissipates heat, lower friction, and formation of tribo-layer on the workpiece surface that lowers the friction effect over time period in machining. A recent study has discussed the tremendous advantages of 1.25 vol% of hybrid nanofluids (alumina-MWCNTs) regarding the cutting forces and surface roughness measurement. Authors have reported high thermal conductivity, viscosity, specific heat ratio, and relatively less density than only alumina or base fluids. Regarding the application of hybrid nanofluids in machining, 20% less main cutting force and 33.4% less surface roughness have been mentioned compared to only $Al_2O_3$ nanofluids [22].

The principal objective of this research study is to investigate the effect of hybrid nanofluids ($Al_2O_3$-MWCNTs) dispersed in vegetable oil-based MQL parameters to model and optimize simultaneously the MQL-associated parameters in milling of Ti-6Al-4 V to improve the machinability. Taguchi-based $L_{16}$ orthogonal array was applied to design the experiments. The fluid concentration, flow rate, and air pressure were varied to investigate their effect on cutting forces, temperature, and surface roughness.

## 2 Experimental details

In this experimental study, milling experiments were performed on Ti-6Al-4 V alloy under hybrid nanofluids-based MQL technology. Besides, the effect of cutting conditions and concentration of fluid (wt.%), flow rate (mL/h), and pressure (MPa) are considered critical parameters. The performance measures such as milling force, temperature, and surface quality were investigated under MQL technology.

### 2.1 Workpiece and cutting tool specifications

To investigate the performance of hybrid nanofluids under machining Ti-6Al-4 V, constant cutting conditions of cutting speed (100 m/min), feed per tooth (0.02 mm/tooth), a width of cut (0.4 mm), and depth of cut (0.5 mm) were used through the experimentation to remove the uncertainty. The levels of the variable parameters were determined through a series of trial tests and recommendations from the tool manufacturer. The workpiece is a Ti-6Al-4 V alloy with dimensions of 150 × 80 × 50 $mm^3$ and is prepared for experimentation in Fig. 2a. The energy-dispersive X-ray spectroscopy (EDS) analysis was done on workpiece material to determine the elemental composition and distribution of chemical elements depicted in Fig. 2b.

Before experimental runs, the grinding process was performed to remove the outer oxide layer. The solution 20% and 5% of nitric acid and hydrofluoric acid were used to take off the layer of the heat-affected zone. The chemical composition and thermo-physical properties of Ti-6Al-4 V are provided in Table 1.

The CNC milling (model, Mikron UCP-710), having a maximum of 20,000 rotations per minute (RPM) and motor power of 13.4 kW, was used to perform the experiments. The FIRE-cemented coated carbide cutting tools (manufactured by Guhring; types, 3629) are reported as an ideal due to high hardness, toughness, wear resistance, and excellent performance even at high temperatures [11]. The coating (3300HV) was used due to high oxidation temperature and hardness, good thermal resistivity, and adhesion with poor frictional coefficient and thermal conductivity [23]. The diameter of the cutting tool is 8 mm, there are four cutting flutes, helix angle is 42°, and tool mill tool length is 63 mm, respectively. Figure 3 depicts the geometric characteristic of the end-mill showing helical length, total length, and helix angle features.

The variable machining conditions (hybrid nanofluids concentration, MQL flow rate, and compressed air pressure) are control factors. MQL flow rate was controlled by the MQL system, and constant air pressure was supplied by a compressor. Based on the number of parameters and levels, a Taguchi-based $L_{16}(4^3)$ orthogonal array is used for the design of experiment. Design Expert 10.0.0$^{(R)}$ was used

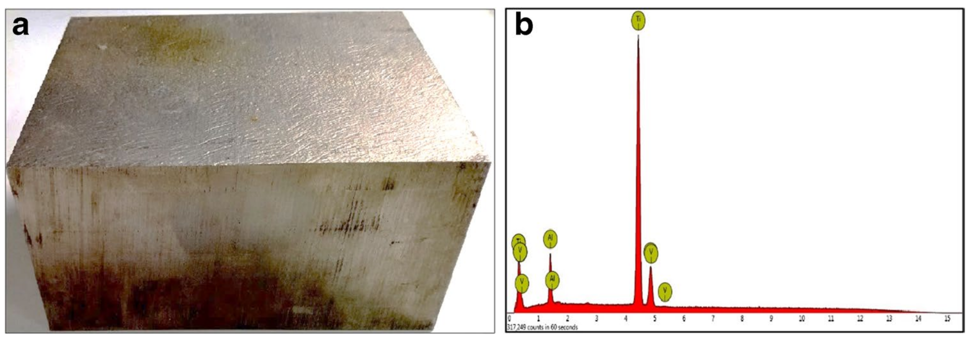


**Fig. 2** **a** The workpiece sample prepared for milling process. **b** EDS analysis of the workpiece

**Table 1** The chemical, mechanical, and thermal characteristics of Ti-6Al-4 V [20]

| Chemical composition of Ti-6Al-4 V | | | | | | | |
|---|---|---|---|---|---|---|---|
| Al | V | C | Fe | O | N | H | Ti |
| 5.5–6.74% | 3.5–4.5% | 0.1% | 0.3% | 0.2% | 0.05% | 0.0125% | Balanced (%) |
| Thermo-mechanical properties of Ti-6Al-4 V | | | | | | | |
| Density | | 4470 kg/m$^3$(at 23 °C) | | Yield strength | 828 MPa (0.2% offset) | | |
| Young's modulus | | 114 GPa | | Elongation | 10% | | |
| Poisson's ratio | | 0.3 (at 23 °C) | | Hardness | 30–34 Rc | | |
| Tensile strength | | 895 MPa | | Specific heat | 560 J/kg°C | | |
| Thermal conductivity | | 7.2 W/m°C | | Melting point | 1649 °C | | |

**Fig. 3** The coated carbide power-mill with geometric characteristics

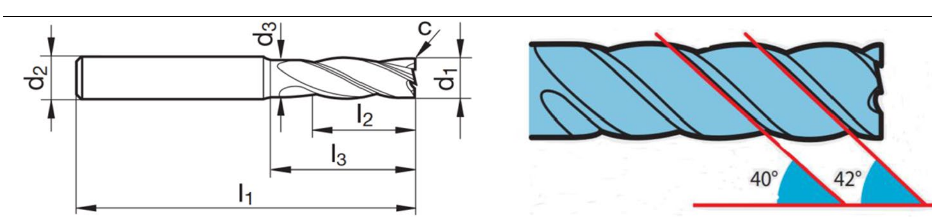


| d1(mm) h10 | d2(mm) h6 | d3(mm) | I1(mm) | I2(mm) | I3(mm) | C(mm×45°) | z | Ø° | Hardness: |
|---|---|---|---|---|---|---|---|---|---|
| 8 | 8 | 7.70 | 63 | 19.0 | 26.0 | 0.15 | 4 | 40~42 | <1300 N/mm$^2$ |

to design the experiments and to perform the analysis of variance (ANOVA), the significance of the model, and the contribution of each parameter. Parameters and their levels were used for a total of 16 experimental runs (Table 2).

## 2.2 Hybrid nanofluids preparation and MQL system

Initially, Blasocut (Vascomill MMS FA-1, Blaser-Swisslube, Switzerland) oil having 5vol% of distilled water was used as base fluid. The hybrid $Al_2O_3$-MWCNTs is finally achieved by mixing 25% of $Al_2O_3$ nano-additives (diameter: 20 ~ 30 nm) and 75% of multiwalled carbon nanotubes MWCNTs (diameter: 30 ~ 50 nm) at different concentrations in the base fluids. There was no surfactant or detergent used in this preparation of hybrid nanofluids, keeping the sustainability perspective during preparations. A fresh hybrid nanofluid sample was prepared for each test and was used immediately to prevent possible sedimentation and/or agglomeration. These nanofluids were ultrasonicated in a digital ultrasonic heater for 3 hours to prepare stable and homogeneous suspension [21] (Fig. 4). The process was repeated in cycles to ensure the fine dispersion of particles without agglomeration and aging after some time or during experimentation.

**Table 2** The minimum quantity lubrication factors and levels

| Variable name | Units | Parameter levels | | | |
|---|---|---|---|---|---|
| | | 1 | 2 | 3 | 4 |
| Nanofluids concentration (conc.) | (wt.%) | 0.06 | 0.12 | 0.18 | 0.24 |
| MQL flow rate ($f_r$) | (mL/h) | 40 | 80 | 120 | 160 |
| Air pressure ($A_p$) | MPa | 0.5 | 0.6 | 0.7 | 0.8 |

The MQL system comprises a compressor, nanofluids reservoir, and an adjustable nozzle. MQL chamber mixes the oil and air sprinkling on the cutting zone. In MQL, an atomizing nozzle is fixed near the cutting zone to supply air-oil (containing hybrid nanofluids) mixture at the tool-chip interface. The adjustable nozzles is 20 mm far from the tool-workpiece contact at an angle of 40° from the workpiece surface.

## 2.3 Responses measurement

Cutting forces in milling are critical characteristics of a process that has a direct relation with the wear of the cutting tool, material hardness, and precision of the machine tool. The Kistler dynamometer was utilized to measure three-dimensional forces such as cutting force, radial force, and feed force. This system amplifies the multi-channel signals, processes the data acquisitions, and displays the force signals ($F_x$ = radial force, $F_y$ = feed force, and $F_z$ = normal force). The sampling frequency of data collection was set as 5000 Hz.

The Fluke-Ti32 thermal infrared camera records images at a rate of 60 Hz using an integration time of 5 s. The infrared spectral bandpass is 8 µm. The emissivity value chosen for Ti-6Al-4 V was 0.95. With the chosen frame rate and optics, the field of view (FOV) is 3.7in diagonal landscapes (640 × 480 pixels). Temperature range is − 20 °C to + 600 °C. SmartView® software was used for analysis. Compensation for reflected background temperature on the Imager set GB = 20.0 in the Background-Tab for the adjustment of the reflected background temperature setting. In thermography, the camera does not directly measure the cutting temperature, but radiation and the black body reference temperature are measured as the base body for calibration. In this study, a black body is used to calibrate the infrared camera between 125 and 500 °C to evaluate the radiant temperature.

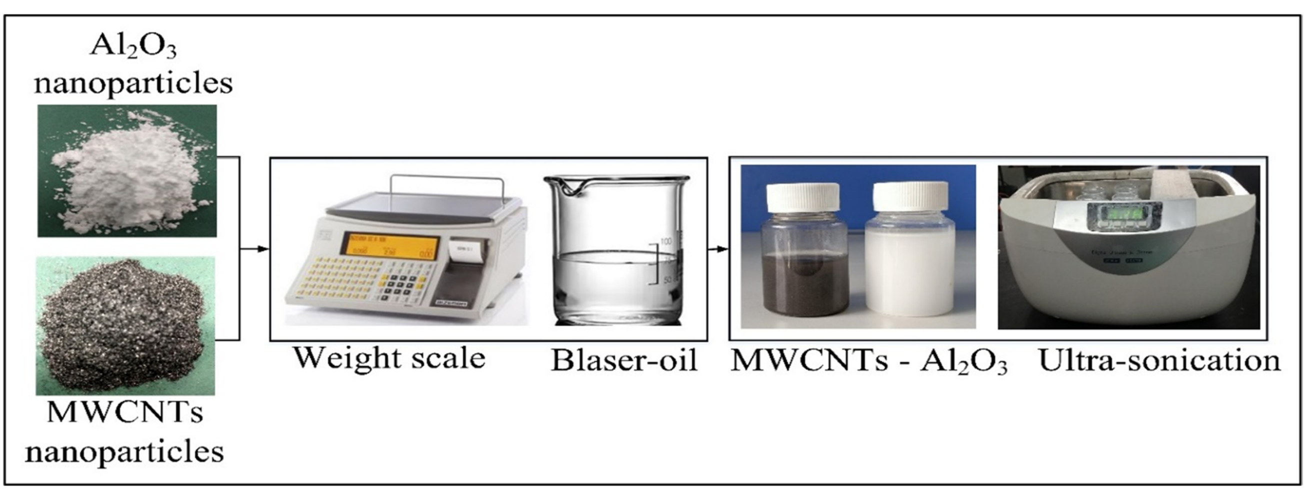


**Fig. 4** Two-step method to prepare hybrid nanofluids

In calibration, the camera is fixed directly to the black body and focused on the plane [24]. The roughness of the outer surface of the workpiece is a standard indicator of the service life of the final product. The surface roughness was measured with the Surf-test (Mahr-1 Perthometer) for a measurement length of 5.6 mm. The workpiece material hardness is a factor that affects the reliability of the final product. The experimental details regarding the cooling system and measuring setup of machining characteristics are illustrated schematically in Fig. 5.

## 3 Results and discussion

In this section, the experimental findings are collected and discussed in detail under different input variables. Taguchi method helps to reduce the variation to achieve targets with the minimum number of experiments. Taguchi is a clear and easier method for analysis of results. Based on the Taguchi method, milling characteristics such as cutting force, cutting temperature, and surface quality were evaluated under the effect of concentration (Conc.), flow rate (fr), and air pressure (Ap). According to Taguchi $L_{16}$ orthogonal array, the experimental results are listed in Table 3. Moreover, the S/N ratio was provided for each response value.

The S/N ratio was calculated through the "less the better" formula using Minitab.18.1$^{(R)}$ software presented in Eq. 1, and outputs were placed in Table 3. In addition, ANOVA for the S/N ratio, having each performance measure, was determined to confirm the model significance as well as an individual variable contribution (Table 4).

It is pertinent to mention that the $P$ value is less than 0.05, depicting that each parameter in the model has a significant contribution to the model. For resultant force $F_R$, coefficient of determination ($R^2$) is 96.65%, adjusted $R^2$ and predicted $R^2$ are closer to each other (difference < 0.2). Similarly, for temperature $T$, $R^2 = 97.7\%$, and surface roughness $R^2 = 96.22\%$, respectively. The mean value of

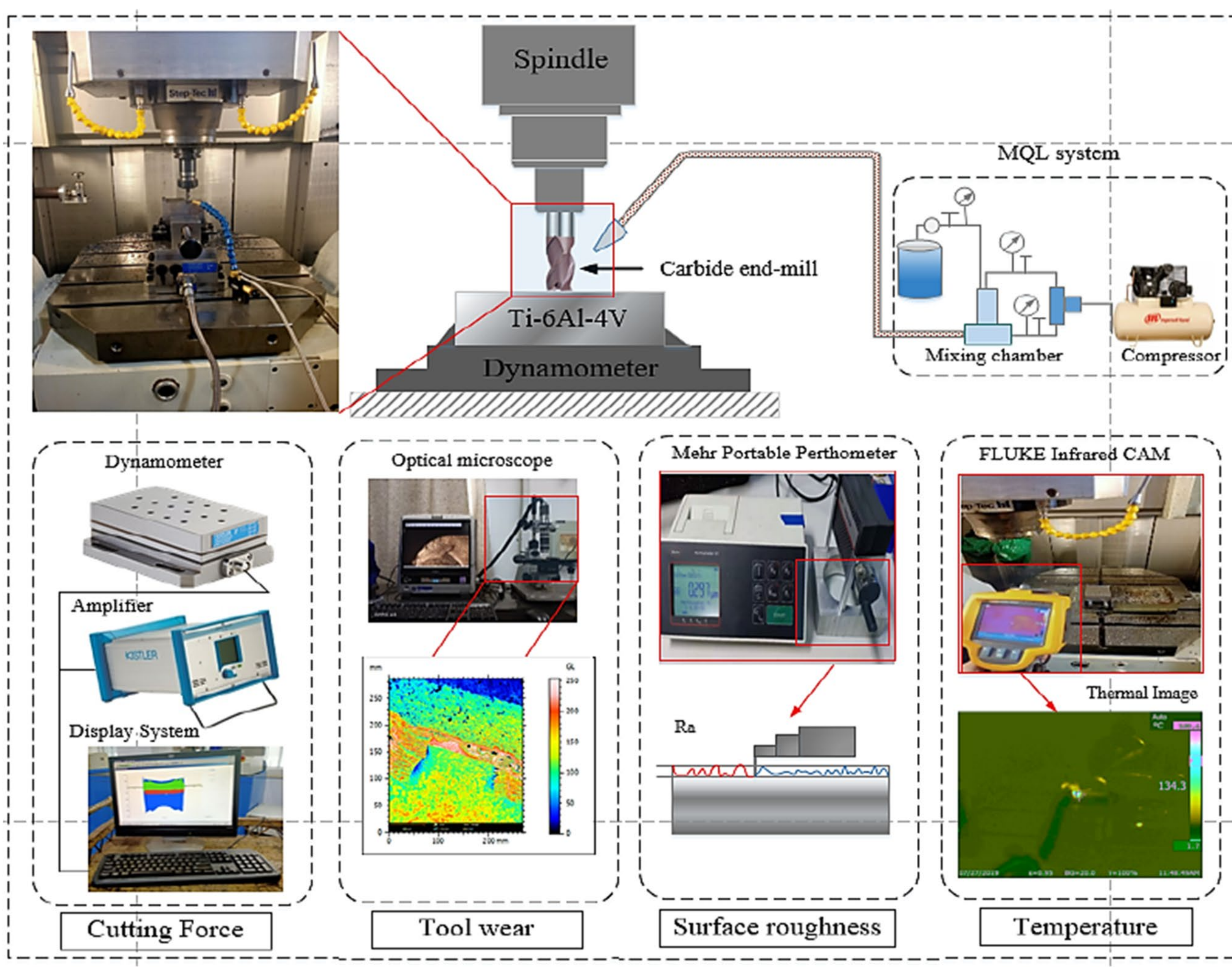


**Fig. 5** Minimum quantity lubrication system for automatic lubrication

**Table 3** Taguchi-based experimental design and measured responses

| Run # | Control parameters | | | Performance measures | | | Signal-to-noise ratios | | |
|---|---|---|---|---|---|---|---|---|---|
| | Conc | fr | Ap | $F_R$ (N) | T (°C) | Ra (μm) | S/N_$F_R$ | S/N_T | S/N_Ra |
| 1 | 0.06 | 40 | 0.5 | 45.73 | 229.34 | 1.38 | −33.20 | −47.21 | −2.80 |
| 2 | 0.06 | 80 | 0.6 | 42.12 | 208.43 | 1.21 | −32.50 | −46.38 | −1.66 |
| 3 | 0.06 | 120 | 0.7 | 33.72 | 178.33 | 1.12 | −30.56 | −45.02 | −0.98 |
| 4 | 0.06 | 160 | 0.8 | 34.15 | 168.21 | 0.97 | −30.67 | −44.52 | 0.26 |
| 5 | 0.12 | 40 | 0.6 | 45.4 | 218.68 | 1.26 | −33.14 | −46.80 | −2.01 |
| 6 | 0.12 | 80 | 0.5 | 36 | 194.81 | 1.21 | −31.13 | −45.79 | −1.66 |
| 7 | 0.12 | 120 | 0.8 | 36.51 | 162.91 | 0.92 | −31.25 | −44.24 | 0.72 |
| 8 | 0.12 | 160 | 0.7 | 27.8 | 159.33 | 0.98 | −28.88 | −44.05 | 0.18 |
| 9 | 0.18 | 40 | 0.7 | 39.45 | 214.35 | 1.18 | −31.92 | −46.62 | −1.44 |
| 10 | 0.18 | 80 | 0.8 | 41.83 | 175.13 | 1.04 | −32.43 | −44.87 | −0.34 |
| 11 | 0.18 | 120 | 0.5 | 25 | 163.83 | 1.05 | −27.96 | −44.29 | −0.42 |
| 12 | 0.18 | 160 | 0.6 | 24.6 | 164.78 | 0.83 | −27.82 | −44.34 | 1.62 |
| 13 | 0.24 | 40 | 0.8 | 43.42 | 195.03 | 0.91 | −32.76 | −45.80 | 0.82 |
| 14 | 0.24 | 80 | 0.7 | 31.6 | 176.84 | 0.76 | −29.99 | −44.95 | 2.38 |
| 15 | 0.24 | 120 | 0.6 | 24.3 | 148.73 | 0.67 | −27.71 | −43.45 | 3.48 |
| 16 | 0.24 | 160 | 0.5 | 26 | 159.82 | 0.57 | −28.30 | −44.07 | 4.88 |

$F_R$ Resultant force, *T* cutting temperature, *Ra* surface roughness

**Table 4** ANOVA of signal to noise based individual response

| Performance measures | | Conc | Fr | Ap | % error | Total sum |
|---|---|---|---|---|---|---|
| $F_R$ | Degree of freedom | 3 | 3 | 3 | 6 | 15 |
| | Seq SS | 10.684 | 39.257 | 6.977 | 1.971 | 58.89 |
| | Adjusted MS | 3.5613 | 13.08 | 2.3255 | 0.3285 | - |
| | *F* value | 10.84 | 39.84 | 7.08 | | |
| | *P* value | 0.008 | 0.000 | 0.021 | | |
| | % contribution | 18.14% | 66.65% | 11.65% | | |
| *T* | Seq SS | 3.03 | 15.51 | 0.5235 | 0.4496 | 19.52 |
| | Adjusted MS | 1.01 | 5.17 | 0.174 | 0.07493 | |
| | *F* value | 13.48 | 69.0 | 2.33 | | |
| | *P* value | 0.004 | 0.000 | 0.174 | | |
| | % contribution | 15.52% | 79.39% | 2.69% | | |
| Ra | Seq SS | 41.5364 | 21.1734 | 0.4779 | 2.4403 | 65.628 |
| | Adjusted MS | 13.8455 | 7.0578 | 0.1593 | 0.4067 | |
| | *F* value | 34.04 | 17.35 | 0.39 | | |
| | *P* value | 0 | 0.002 | 0.764 | | |
| | % contribution | 63.31% | 32.26% | 0.73 | | |

the S/N ratio for each parameter at different levels is exhibited in Table 5.

### 3.1 Cutting temperature under hybrid $Al_2O_3$-MWCNTs MQL

In the process of material removal, most of the heat generates at the primary and secondary shearing zone. The most of heat generated in the workpiece material is due to shear and rubbing, while in the tool material, it is due to friction, rubbing, and distribution of heat at rake and flank face. The quasi-steady-state heat model is normally used to define the heat distribution in the workpiece [25].

$$T_w = \frac{q}{\pi k_w}\int_0^L e^{-\left(\frac{V_{ft(X-a)}}{2\alpha}\right)} K_0\left\{\frac{V_{ft}}{2\alpha}\left[(X-a)^2 + Z^2\right]^{0.5}\right\} f(a)da \quad (1)$$

where $q$ is the frictional or shear heat, $f(a) = (1 + (2a/l_c))$, $K_0$ is the Bessel function,$\alpha$ is the thermal diffusivity of the workpiece, and $L = underformedchipthickness/Sin\varphi$. Therefore, heat generation can be evaluated through this relation. In this place, it is assumed that total heat generation in the

**Table 5** The mean S/N ratio at each parameter level

| Performance measures | Levels | Input variables mean signal-to-noise (S/N) ratio | | |
|---|---|---|---|---|
| | | Conc% | Flow rate | air pressure |
| $F_R$ | 1 | −31.73 | −32.75 | −30.15 |
| | 2 | −31.10 | −31.51 | −30.29 |
| | 3 | −30.03 | −29.37 | −30.34 |
| | 4 | −29.69 | −28.92 | −31.77 |
| $T$ | 1 | −45.78 | −46.61 | −45.34 |
| | 2 | −45.22 | −45.50 | −45.24 |
| | 3 | −45.03 | −44.25 | −45.16 |
| | 4 | −44.57 | −44.24 | −44.86 |
| Ra | 1 | −1.29 | −1.36 | 0.00 |
| | 2 | −0.69 | −0.32 | 0.36 |
| | 3 | −0.15 | 0.70 | 0.03 |
| | 4 | 2.89 | 1.74 | 0.37 |

workpiece and the tool remains equal. The following relation depicts this assumption [26].

$$T_{M_{\text{workpiece-shear}}} + T_{M_{\text{workpiece-rubbing}}} + T_{\text{workpiece-heatloss}} = T_{M_{\text{tool-rubbing}}} + T_{M_{\text{tool-friction}}} + T_{M_{\text{induced flank}}} + T_{M_{\text{induced rake}}} - T_{\text{tool-heatloss}} \quad (2)$$

As MQL is an air-oil mixture impinged on the tool-chip interface, it dissipates heat from the tool and workpiece. Due to oil mixture, the heat losses in $X$, $Y$, and $Z$ directions can be defined as follows [26]:

$$T_{\text{hl}} = \frac{q_{\text{hl}}}{2\pi k_{\text{t}}} \int_0^{\text{Lc}} \int_{-w/2}^{w/2} \left[ \frac{1}{R_{\text{i}}} + \frac{1}{R_{\text{i}}'} \right] d_{\text{y}} d_{\text{x}} \quad (3)$$

$R_{\text{i}} = \sqrt{(X-x)^2 + (Y-y)^2 + z^2}$ ; $R_{\text{i}}' = \sqrt{(X-(2L-x)^2 + (Y-y)^2 + z^2}$ ; and $q_{\text{hl}} = h(T_{\text{tool}} - T_{\text{fluid}})$ $h$ = heat transfer coefficient.

During the milling process, the temperature was measured with the Fluke infrared camera fixed at an appropriate distance from the tool-workpiece interface. Temperature measurement depicts the peak temperature for each milling pass. The measured temperature under dry and MQL hybrid nanofluids mist was displayed in Fig. 6.

Accordingly, the maximum temperature under dry conditions is 372 °C, while under MQL hybrid nanofluids, it is 183 °C. In addition, at different MQL parameters, the temperature was collected and plotted in Fig. 7. Figure 7a demonstrates the S/N ratio of temperature at different levels of nanofluids concentration, Conc (wt%); flow rate, fr (mL/h); and air pressure, Ap (MPa). As the criteria defined for temperature are "less the better," that is why the flow rate has provided less S/N ratio of temperature at high and low levels of temperature. It is valuable to emphasize that the flow rate was the most significant parameter affecting temperature, followed by concentration and air pressure, respectively. This temperature reduction can be associated with the appropriate lubrication of hybrid nanoparticles that increased the cooling capacity, and efficiently dissipated heat from the cutting zone, and controlled the cutting temperature. Due to the high wettability of multiwalled nano-additives, it formed a shielding layer of nanoparticles and reduced friction. In addition, various sized nanoparticles having high heat-carrying capacity lowered the cutting temperature [27]. That is why a high flow rate of MQL has reduced the temperature efficiently. Figure 7b shows the 3D surface plot of temperature under simultaneous variation of concentration and flow rate. The temperature was decreased with the increase of the concentration and flow rate at all the levels of the parameters. It is worthy of mentioning that the lowest temperature was 148 °C at the highest levels of the concentration and flow rate. The key reason behind the significant reduction of temperature is that the high flow rate and nanofluids concentration have extended capacity to absorb the tool-chip heat through $Al_2O_3$-MWCNTs particles. The high heat absorption of hybrid nano-additives also dissipates heat quickly from the cutting region to chip or fluid, as only MWCNTs have almost 150% higher thermal conductivity than the base fluid. So, MWCNTs show better performance regarding the heat transfer properties [28]. Figure 7c shows the

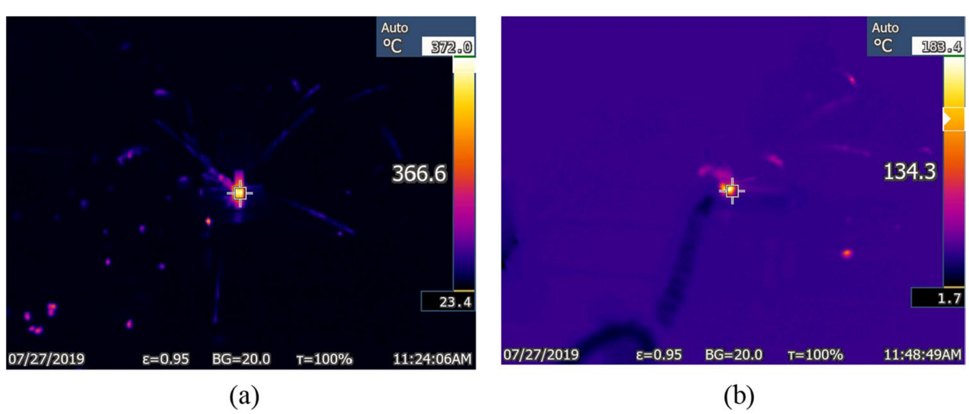


**Fig. 6** Temperature under **(a)** dry and **(b)** MQL hybrid nanofluids

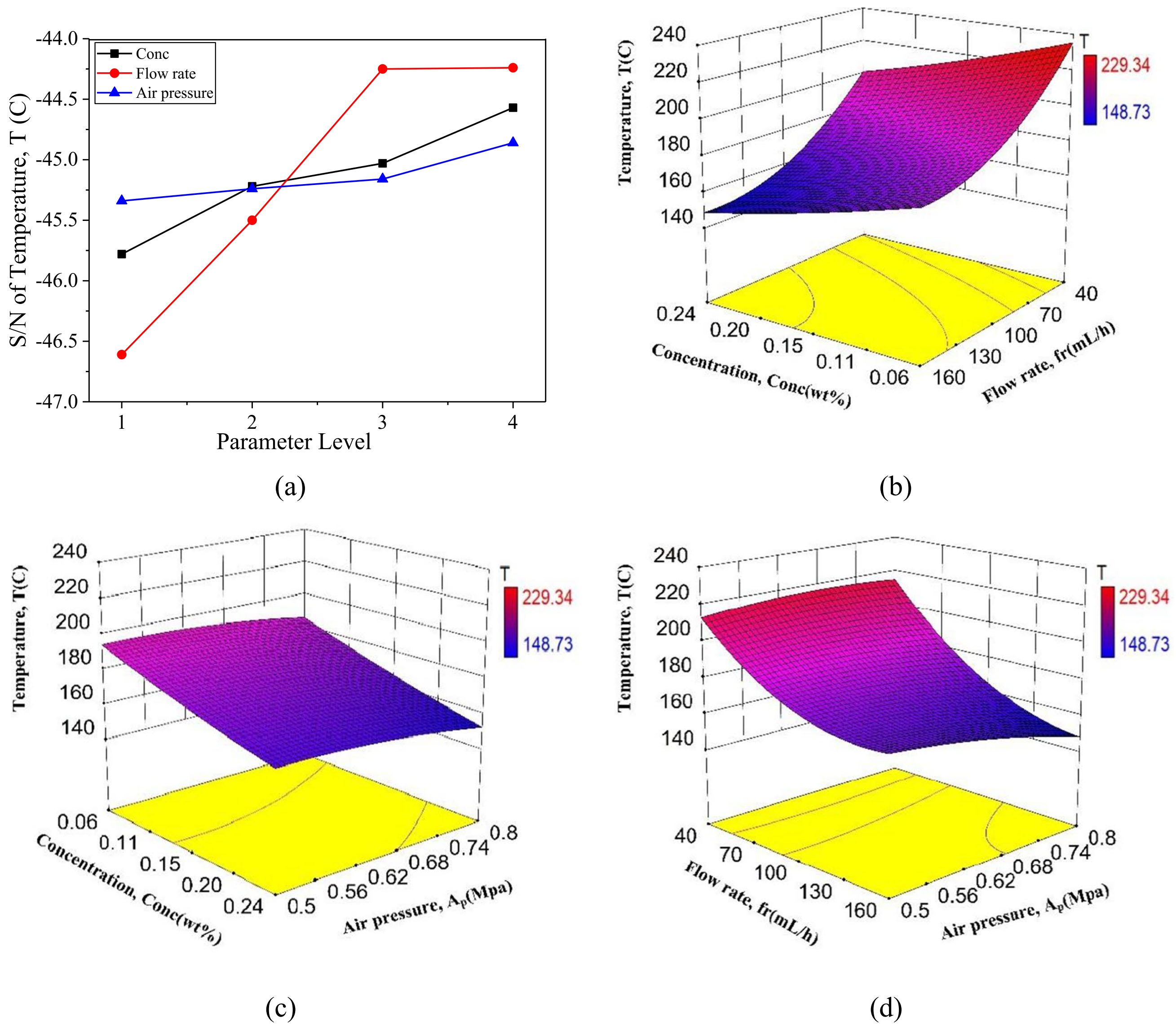


**Fig. 7** **a** S/N ratio of temperature T, 3D surface plot of **b** Conc (wt%) vs. $f_r$ (mL/h), **c** Conc (wt%) vs. $A_p$ (MPa), **d** $f_r$ (mL/h) vs. $A_p$ (MPa)

simultaneous effect of concentration and air pressure on the milling temperature. The cutting temperature was decreased with increasing concentration and air pressure. The lowest temperature (152 °C) was achieved at the highest levels of concentration and air pressure. The reduction in temperature can be attributed to the better morphology, and differently sized nano-additives penetrated well at the cutting zone and dispersed in the base fluid due to weak van der Waals forces, and higher wettability has extracted heat well. Also, due to high pressure, the evaporation phenomenon to dissipate heat was prominent. This phenomenon had effectively prevented the elevation of temperature in the cutting zone. Figure 7d shows the 3D surface plot of temperature under the simultaneous effect of flow rate and air pressure. The temperature was reduced by increasing flow rate and air pressure. The higher flow rate added more nanofluids-assisted fine mist at high air pressure. In the process of the fine penetration of hybrid nanofluids, the spherical and cylindrical shapes of nanoparticles have taken advantage to behave like spacers at the tool-chip interface to directly touch the tool to workpiece surface ultimately reducing the frictional heat generation. Considering the advantages of vegetable oils, fine droplets of vegetable oil having a polar nature align themselves on the surface of the workpiece, forming a thin lubrication film providing adequate lubrication compared to the non-polar nature of cutting oils. Therefore, MQL with vegetable oil has reduced the frictional temperature by applying hybrid lubri-cooling.

### 3.2 Resultant cutting force under hybrid $Al_2O_3$-MWCNTs MQL

The cutting force is very useful in engineering for machine designs and machining settings, although the resultant average force is not the maximum value in the milling process [29]. As the end-mill contains several teeth to cut the material simultaneously, the average cutting force per teeth per cut in *x*, *y*, and *z* direction (refer to Fig. 8) is:

$$\begin{aligned} F_{XT} &= \sum_{i=1}^{z_c} \delta(\mathrm{i}).F_{xi}(\psi_i) \\ F_{YT} &= \sum_{i=1}^{z_c} \delta(\mathrm{i}).F_{yi}(\psi_i) \\ F_{ZT} &= \sum_{i=1}^{z_c} \delta(\mathrm{i}).F_{zi}(\psi_i) \end{aligned} \tag{4}$$

while $\psi_i$ is cutting angle, $z_c$ = number of teeth cutting simultaneously (can't be rounded off), and $z_c = \frac{z \times \psi_s}{360}$, $z$ depicts the number of teeth of the end-mill, $\psi_s$ is swept angle ($\psi_s = \psi_2 - \psi_1$).

$$\delta(\mathrm{i}) = 1 \;\text{ when }\; \psi_1 \le \psi \le \psi_2, \delta(\mathrm{i}) = 0 \;\text{ if }\; otherwise$$

$F_{XT}$, $F_{YT}$, and $F_{ZT}$ are the average force per tooth in *x*, *y*, and *z* directions. The resultant force $F_R$ was determined through the formula of total force *F*:

$$F_R = \sqrt{F_x^2 + F_y^2 + F_z^2} \tag{5}$$

Here, $F_x$ depicts the radial force component, $F_y$ shows the feed force component, and $F_z$ shows the normal force to the workpiece surface. The resultant milling force consists of elements induced due to the involved mechanism of the machining process.

Figure 9a demonstrates the S/N ratio of the resultant force under variation of concentration, Con (wt%); flow rate, fr (mL/h); and air pressure, Ap (MPa). It can be seen from Fig. 9a that the S/N ratio of resultant force $F_R$(N) is smaller at the low levels of concentration and flow rate, and it increases by increasing the concentration and flow rate. However, the S/N ratio of $F_R$ is higher at low levels of air pressure and decreases at the highest level of air pressure. The smaller the S/N ratio of $F_R$, the better, so by increasing the concentration and flow rate, the resultant force $F_R$ was decreased. While increasing air pressure, the resultant force $F_R$ was slightly increased; however, the effect of air pressure was not so high on the effect of the resultant force. Figure 9b depicts the 3D response surface plot underscoring the simultaneous effect of concentration and flow rate on resultant force $F_R$. The resultant force $F_R$ decreased with the increase of concentration and flow rate. However, the effect of flow rate on the reduction of resultant force $F_R$ was significantly higher than that in concentration.

The highest resulting force $F_R$ was 24 N at the highest level of concentration and flow rate. The effectiveness of nanofluids concentration and flow rate towards the reduction of resulting force $F_R$ can be associated with the addition of hybrid nanoparticles provided lubrication due to a ball-bearing effect at the cutting zone. The suspended hybrid nano-additives of spherical and cylindrical shapes in Blaser oil form a thin layer of lubrication that reduces friction between the tool-chip interface. The high flow rate has more ability to prevent direct contact of end-mill with the workpiece surface from lowering down the cutting forces [30]. Figure 9c shows the simultaneous effect of concentration and air pressure on the resulting force $F_R$. The resulting force $F_R$ was decreased with the increase of concentration and slightly increased with the increase of the air pressure. The lowest resulting force $F_R$ of 25 N was achieved at a high level of concentration and the lowest level of air pressure. It is important to mention that a slight increase in $F_R$ was due to the nozzle angle (about 65°) that directly put air pressure on the tool-chip interface and compressed the workpiece below. That may be one of the possible reasons behind a slight increase in the resulting force. Figure 9d underscores the 3D response surface plot of flow rate and air pressure. The resulting force $F_R$ is decreased with the increase of flow rate and increased with the increasing air pressure. The high flow rate of MQL fine mist contains a high proportion of nano-additives suspended in Blaser oil which behaves as a polar nature coolant. The molecules of oil align themselves in opposite charge poles. These strong polar bonds and suspended nanoparticles reduce friction significantly. In addition, the higher wettability and viscosity allow the fine mist to stay longer on the workpiece and tool surfaces. The nano-additives penetrate

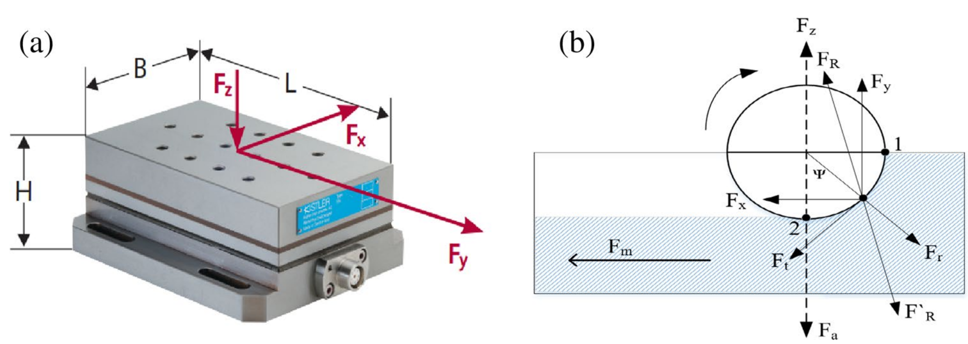


**Fig. 8** **a** Force components $F_x$, $F_y$, and $F_z$ on a dynamometer. **b** The force components in the milling process [29]

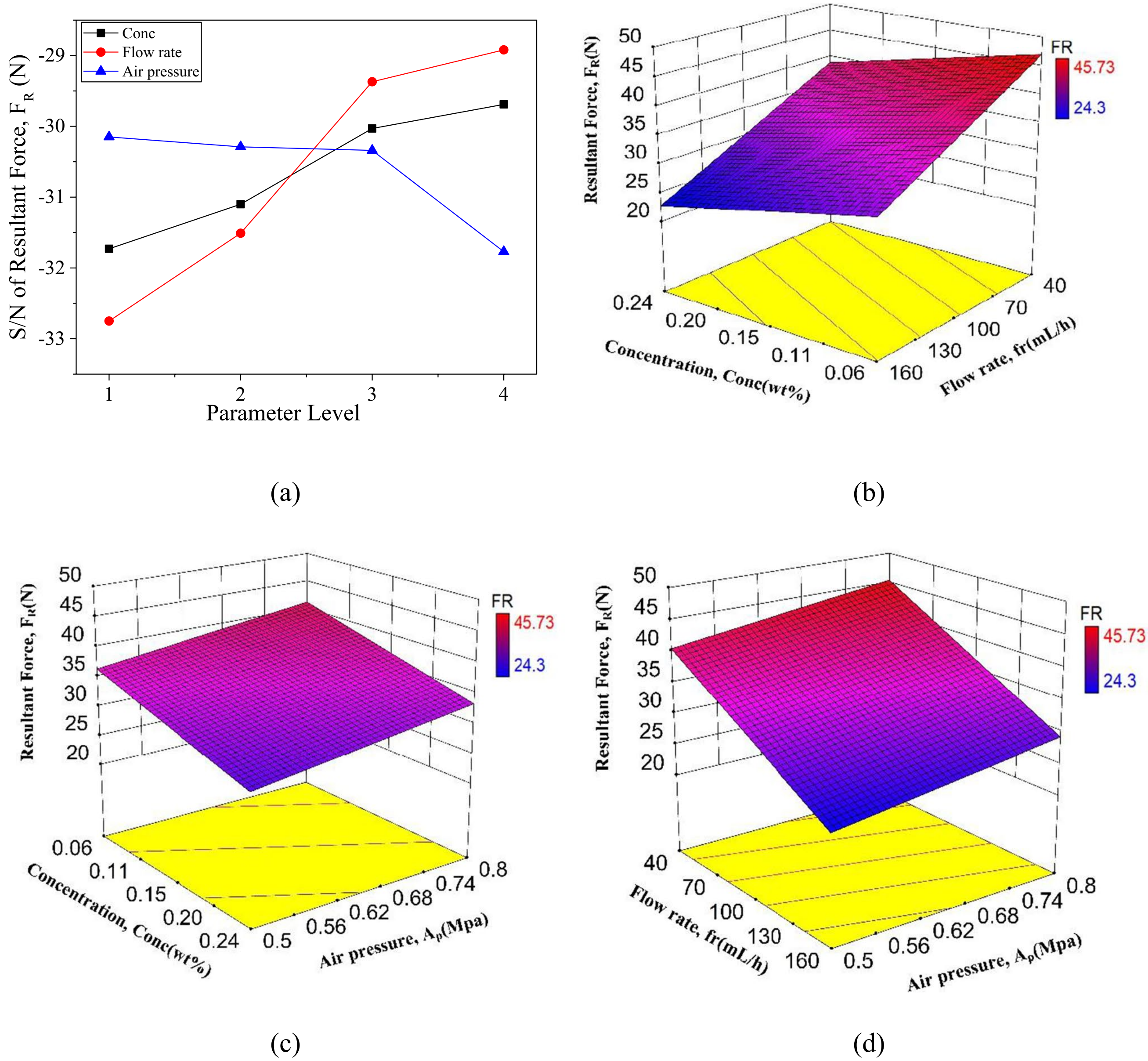


**Fig. 9** **a** S/N ratio of resultant force $F_R$, 3D surface plot of **b** Conc (wt%) vs. $f_r$ (mL/h), **c** Conc (wt%) vs. $A_p$ (MPa), **d** $f_r$ (mL/h) vs. $A_p$ (MPa)

well into the tool-chip interface. The MWCNTs have layered structures of carbon that behave as a lubricant, while the spherical shape of the $Al_2O_3$ nano-additives shows a rolling effect reducing the friction and cutting forces.

### 3.3 Surface roughness under hybrid $Al_2O_3$-MWCNTs MQL

The arithmetic average height parameter ($R_a$), also named CLA (center-line average), is the most frequently used roughness parameter for quality control. For a specific length of the sample, the average irregularities/deviations from the mean line are named as an average surface roughness ($R_a$). The $l_r$ is the measurement length, $l_n$ is the necessary length for measurement, and $h_i$.....$h_n$ are the absolute distance of each point from the mean line. The equation for the arithmetic mean height can be defined as follows:

$$R_a = \frac{1}{l}\int_0^1 |h(x)|.dx \tag{6}$$

$R_a$ = average height (μm); $l$ = number of intersections of the profile.

Figure 10a shows the surface plots of the S/N ratio of surface roughness corresponding to the simultaneous effect of concentration, flow rate, and air pressure. The S/N ratio of surface roughness increased with the increase of concentration, flow rate, and air pressure; however, the concentration of nanofluids affected the S/N ratio of surface roughness considerably at the high level. Figure 10b illustrates the 3D response of the concentration and flow rate on the surface roughness. The surface roughness decreases with the increase of the concentration and flow rate; however, the surface roughness is more sensitive to concentration than the flow rate. The minimum surface roughness with 0.57 µm was achieved at the maximum level of concentration and flow rate. The significant effect of the nanofluids of concentration on the surface roughness can be referred to as the tribological properties of MWCNTs. Although there are no research findings regarding the tribological superiority of MWCNTs over $Al_2O_3$, it is claimed that MWCNTs are better lubricants than $Al_2O_3$. As the MWCNTs are carbon particles, superior surface area and their structure can sustain high pressure and fill the micro-spaces on the workpiece surface. In this way, the surface finish was improved under the high concentration of hybrid nanofluids. Figure 10c shows the simultaneous effect of concentration and air pressure on surface roughness. It is identified that surface roughness was decreased with increasing concentration and air

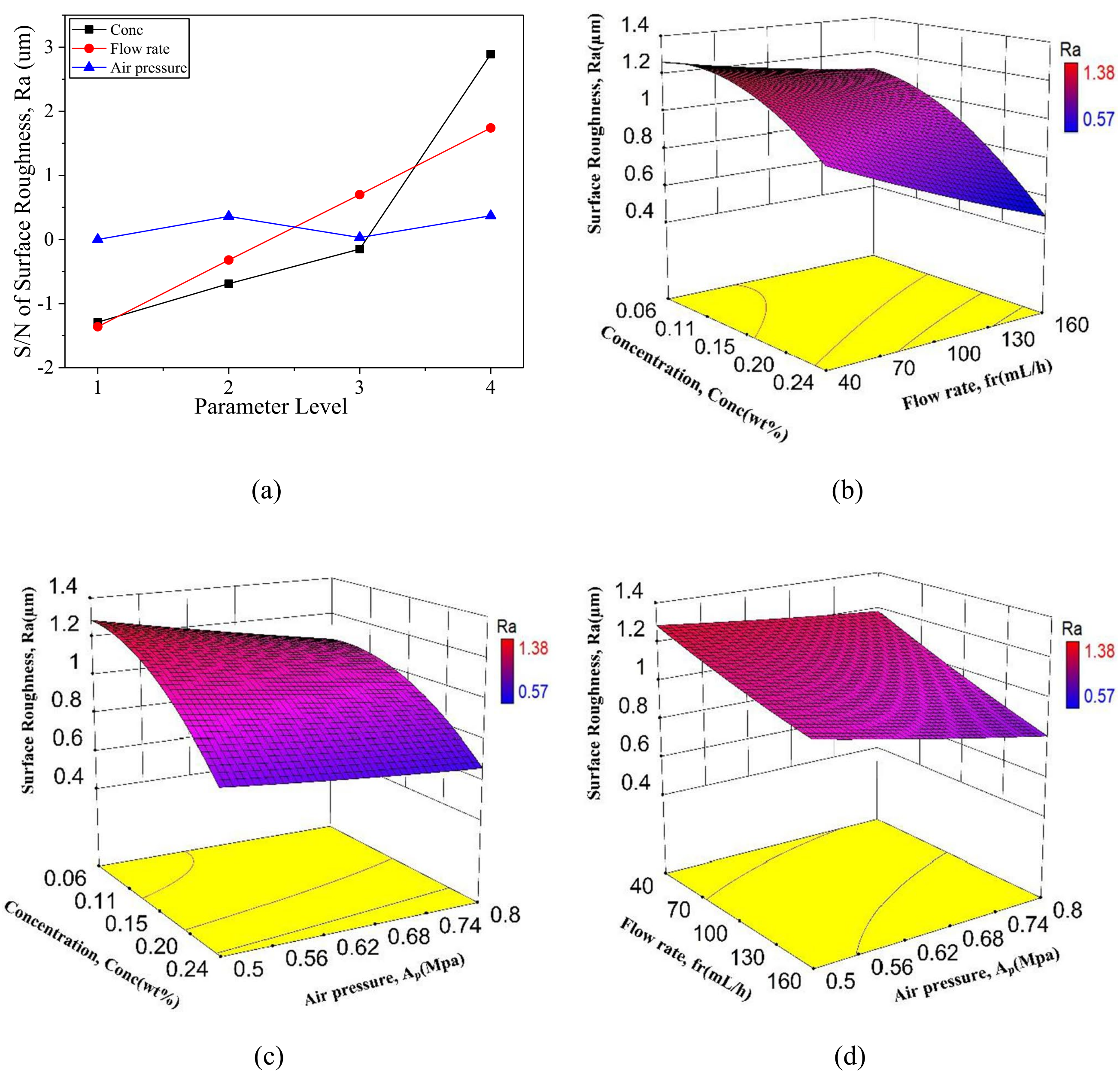


**Fig. 10** **a** S/N ratio of temperature Ra, 3D surface plot of **b** Conc (wt%) vs. $f_r$ (mL/h), **c** Conc (wt%) vs. $A_p$ (MPa), **d** $f_r$ (mL/h) vs. $A_p$ (MPa)

pressure; however, surface roughness was more dependent on concentration than the air pressure. The minimum surface roughness of 0.64 μm was achieved at the highest level of nanofluids concentration and air pressure. Figure 10d underscores the effect of flow rate and air pressure on the surface roughness. The surface roughness was decreased with the increase of flow rate and air pressure. This phenomenon can be associated with the cooling/lubrication characteristics of the hybrid nanofluids, extended the wettability, stayed longer on the tool cutting edge, dissipated heat, and provided lubrication as discussed by the earlier studies [31]. This mist can penetrate and form a tribo-film on the surface of the tool and the workpiece and decrease the coefficient of friction. Accordingly, the hybrid nanofluids under high flow rates behave like rolling, polishing, and filming actions to fill the empty spaces on the workpiece surface. That is why hybrid nanofluids having spherical shaped $Al_2O_3$ [32] and cylindrical MWCNTs in different sizes provide the synergistic on workpiece surface than single nanofluids [33].

### 3.4 Tool wear under hybrid $Al_2O_3$-MWCNTs MQL

The cutting forces and temperature are mostly influenced by the wear of the cutting tool. The wear of cutting tools depends upon tool materials, type of coatings, cutting conditions, and cooling/lubrication [34]. In this section, the effect of nanofluids-assisted MQL associated parameters (concentration, flow rate, air pressure) were studied to explore the effect of hybrid nanofluids MQL on tool wear behavior. The % concentration, flow rate, and air pressure are fixed as 0.24 wt%, 120 mL/h, and 0.6 MPa, respectively. The state of the cutting tool was highlighted through scanning electron microscopy (Fig. 11). The dominant wear patterns under MQL are abrasive wear, coating peeling, and chip adhesion. From Fig. 11, it can be determined that less severe abrasive wear was observed between the cutting tool and the workpiece. Besides, coating peeling was appeared due to chip sliding on the tool surface and the formation of saw tooth chips and BUE during cutting. Ezugwu et al. [35] have reported BUE formation on the cutting tool in the machining of hard-to-cut materials which is one of the issues encountered during cutting. It can be said that when the cutting temperature reaches a critical stage, the tendency of chip welding becomes high enough owing to the chemical closeness between workpiece material and cutting tool material Fig. 12.

As the cutting tool starts cutting, due to poor thermal conductivity of Ti-6Al-4 V, cutting tool scratches lead to thermal cracks initiation on the cutting edge due to imbalanced heat and fatigue on different portions of the cutting tool. As the cutting tool continues to cut, thermal crack energy starts accumulating. When the thermal crack energy exceeds the crack propagation threshold, it enables thermal cracks initiation. As a result, this phenomenon lowers the coating thickness, reduces its strength, and accelerates coating peeling [36]. The mist carrying hybrid nano-additives penetrated well at the tool-chip interface due to air pressure and formed a tribo-film. It significantly reduced the severe edge chipping, coefficient of friction, and adhesion from the tool cutting edge. These advances with superior lubrication/cooling allowed chip adhesion and coating peeling to occur in a smaller area of the cutting edge. The reduction of such severe chipping may occur due to nano-additives behaving as spacers between tool-workpiece interface and prevented direct tool contact, helped to slip the chip on the cutting edge rather than adhesion.

### 3.5 Surface topography and chip morphology

The surface topography of the machined workpiece is highlighted in Fig. 12. It is obvious that hybrid nanofluids MQL conditions have generated a smooth surface, with fewer peaks and valleys. It can be attributed to the smooth wear of the cutting tool and less chip adhesion and welding under hybrid nanofluid conditions. The feed marks were appeared on the surface owing to the interaction of the current tool path with the neighboring tool paths. Thus, the feed marks were blurred, and an increase in feed is marked with increasing the workpiece length. However, very fewer chips sticking on the newly generated surface were observed because the pressured mist has flown away from the chips.

Chip morphology analysis is presented to relate the surface quality and material behavior under machining. Although a different type of chips are produced in the machining of different materials, however, coolings/lubrications have also a significant effect on the shape of chips. For example, machining of Ti-6Al-4 V provides discontinuous and saw-tooth chips. The chip analysis defines the tool-chip contact length, friction at the common interface, and ultimately the heat generation at the secondary shearing zone. These heat generation and friction have a key role in the final shape of chip formation. The chip consisted of localized shear bands, formed by phase change (dynamic recrystallization) due to exceeding thermal softening from strain hardening. The application of MQL also produces varying chip morphologies rather than varying chip thickness and serration distances. Figure 13 depicts the saw-tooth and discontinuous chips at a closer view of chips having adiabatic shear bands. However, the backside of the chip underscored feed marks of shearing material in the feed direction of the cutting tool. The less severe feed marks (friction tracks) indicated the tribo-film formation, and rolling effects under hybrid nanofluids restricted these marks.

The energy-dispersive X-ray spectroscopy (EDS) analysis has underscored Ti, V, and Al components of chip analysis.

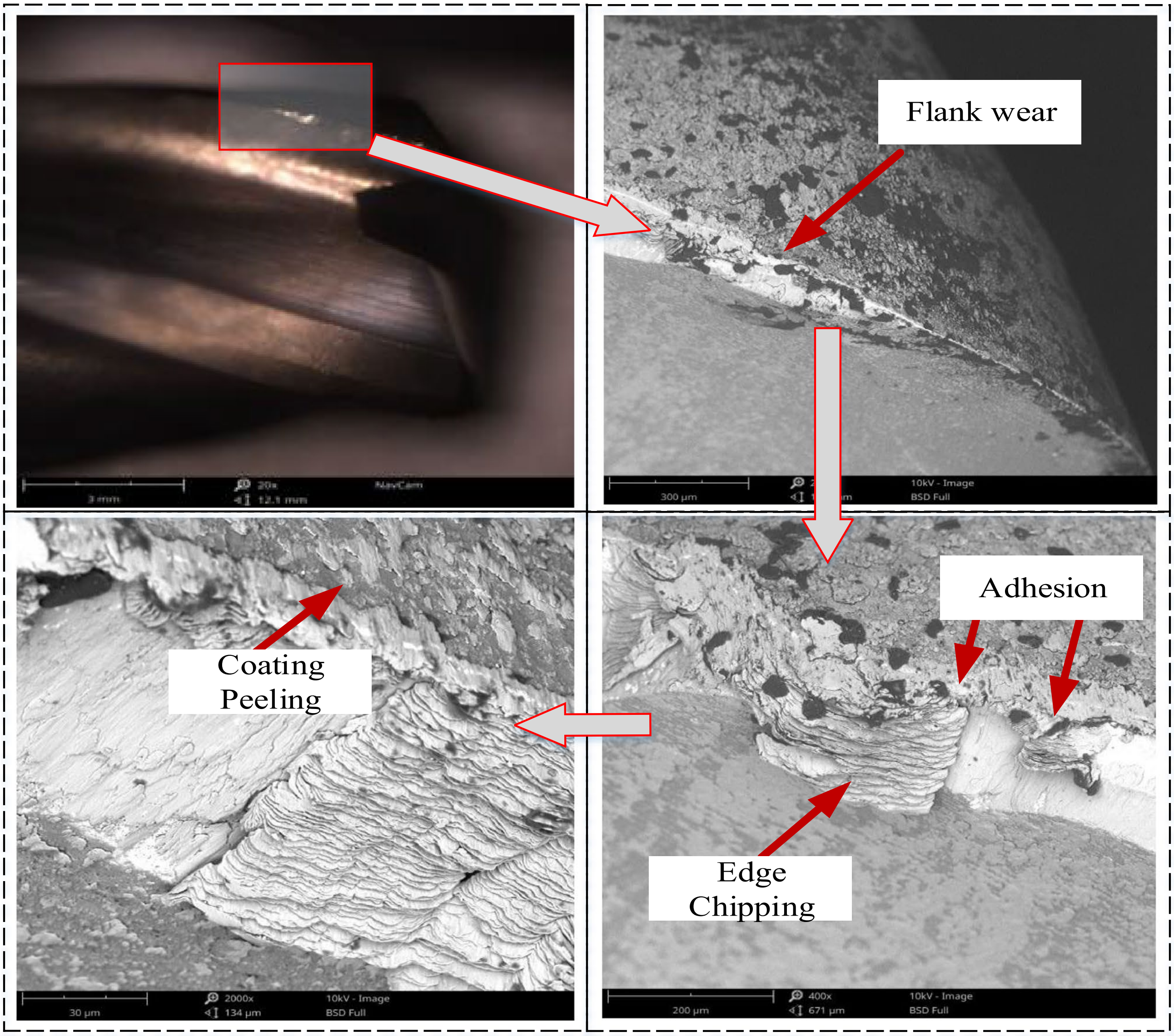


**Fig. 11** The SEM analysis of the milling tool under 0.24 wt% concentration, 120 mL/h flow rate, and 0.6 MPa air pressure

To prevent the heat or transfer heat from the tool-chip interface, hybrid nanofluids MQL is expected to dissipate heat from the cutting region. In this way, it limits the thermal softening of the workpiece material and eases chip flow by the presence of nano-additives at the tool-chip interface. In addition, the pressured nano-mist dissipated the generated heat and prevented chip welding which facilitates the chip flow, and that is owing to the presence of MWCNTs nano-additives. Also, due to the uniform strain on the material during cutting (i.e., low and high strain leads to the formation of saw-tooth chips), wider and lower in-depth saw-tooth was observed under MWCNTs-assisted MQL.

### 3.6 Hybrid ($Al_2O_3$-MWCNTs) nanofluids mechanism

Several researchers have reported the superior thermal, physical, and rheological properties of hybrid nanofluids than single nanofluids in turning, milling, drilling, and metal forming [17, 37]. The improved cutting conditions for the machining of difficult-to-cut materials are attributed to the hybrid nanofluids owing to thermal conductivity and lubrication to limit the heat and wear of the cutting tool. The variable sizes and shapes of the nanoparticles suspended in base fluid provide significant advantages during the cutting process. Also, understanding the possible mechanisms is highly essential (Fig. 14).

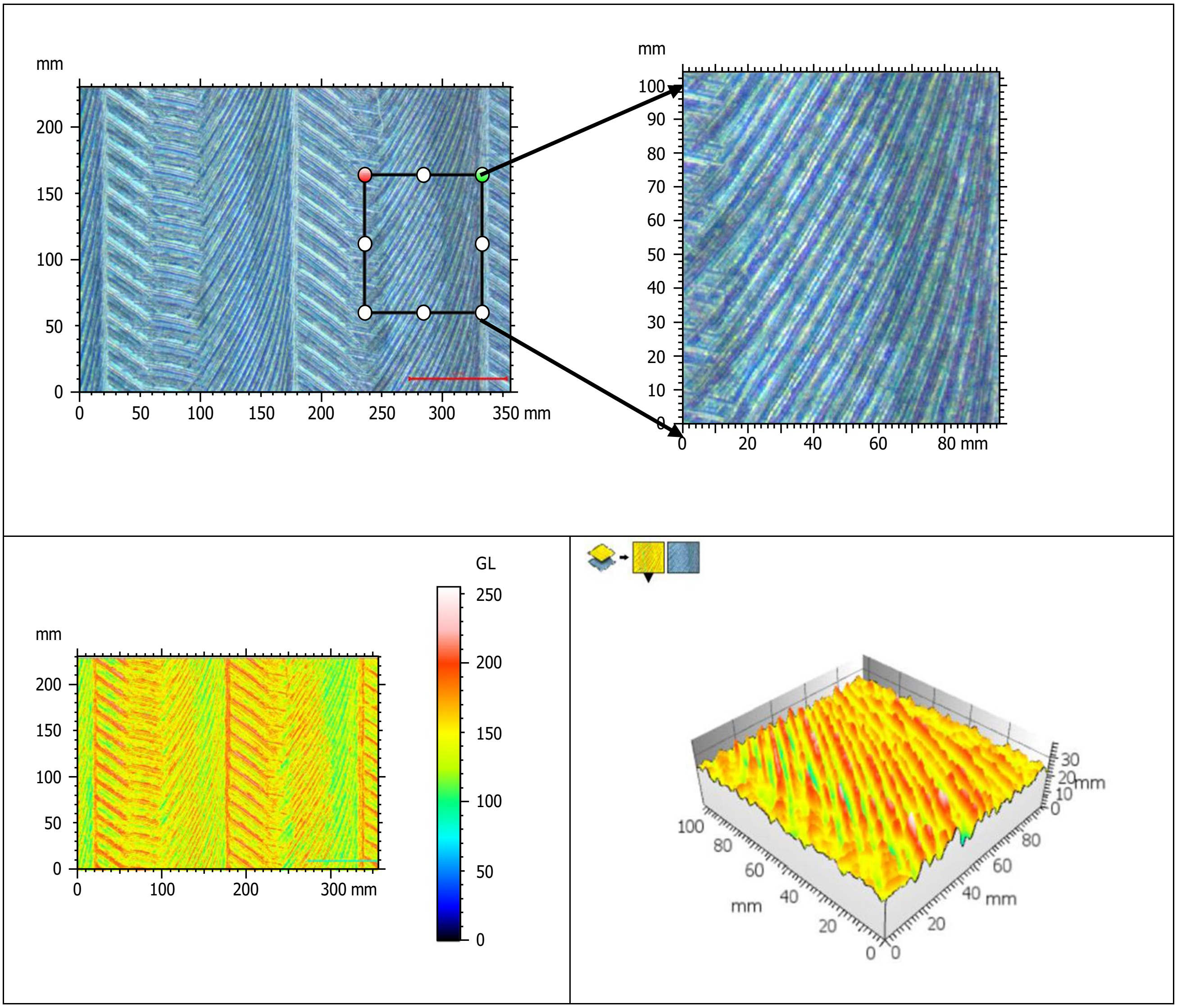


**Fig. 12** Surface topography of the machined surface at nanofluids concentration of 0.24vol% and 120 mL/h of flow rate at 0.6 MPa of air pressure

The possible mechanisms of hybrid nanofluids are summarized as follows:

- By mixing hybrid nanofluids and compressed air (60:40) in a mixing chamber, a very fine mist is generated by atomizing through an MQL nozzle.
- The resultant fine mist consisted of multiple-sized hybrid nano-additives surrounded by a thin oil film. This mist (multiple-sized) has the opportunity to penetrate well in the cutting zone due to the difference in momentum and pass through the tool pores.
- Thus, hybrid nanofluids mist forms a dipolar thin film on the tool and workpiece surface to enhance the tribological characteristics and less friction. The superior thermal conductivity and lubrication capability of $Al_2O_3$-MWCNTs reduce the heat and friction.
- Hybrid nano-additives behave as excellent spacers and ball-bearing to different shape and size to limit the rubbing contact of tool to the workpiece. The concentration of hybrid nano-additives allows enhancement at the tool-workpiece interface. Hybrid nanofluids with multiple-sized nano-additives filled micro-voids on the workpiece surface due to pressure mist resulting in improving the surface finish.

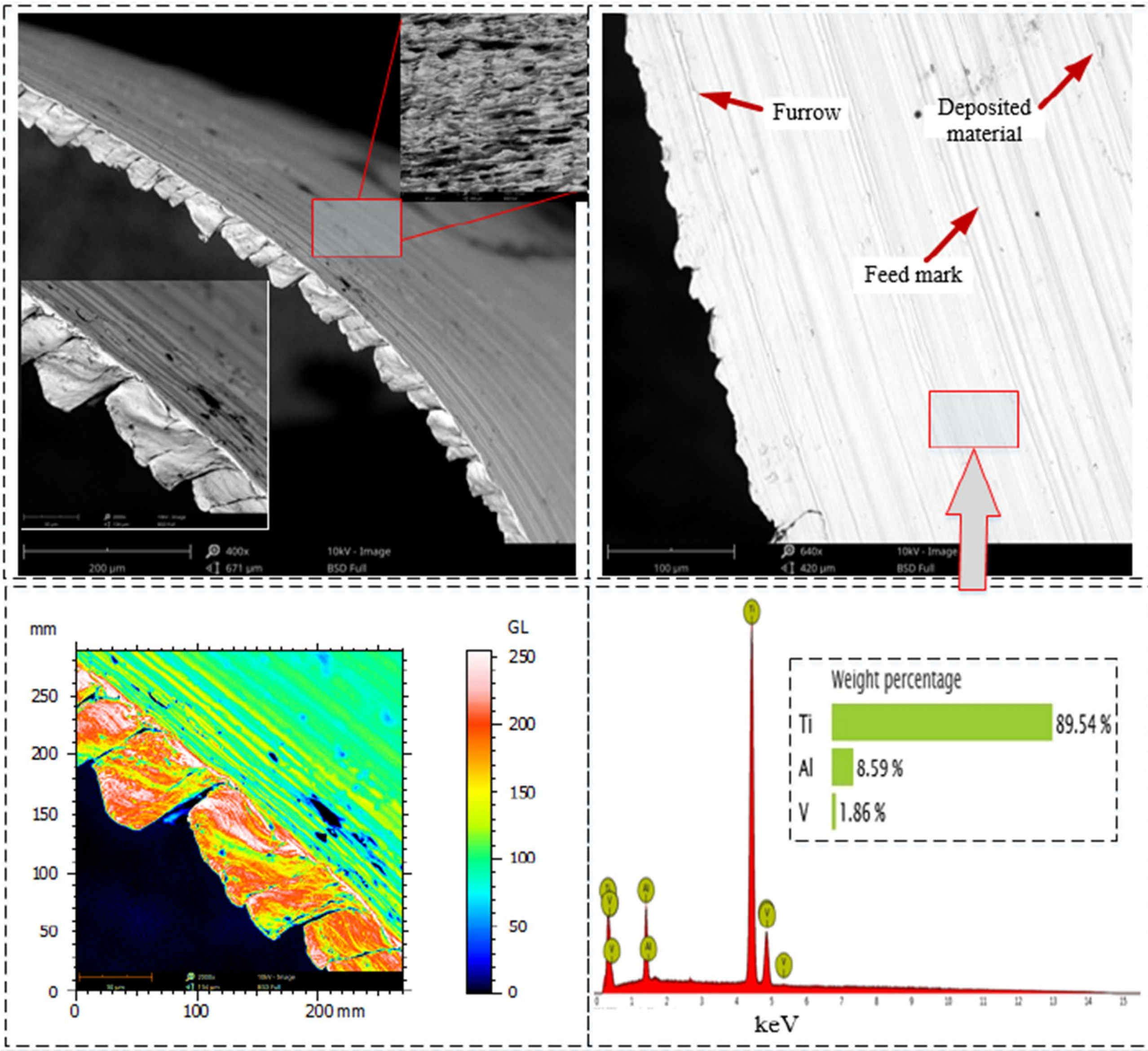


**Fig. 13** The SEM analysis of chip and EDS of the chip produced under MQL machining at a nanofluids concentration of 0.24vol% and 120 mL/h of flow rate at 0.6 MPa of air pressure

## 4 Conclusion and future work

In this research work, the milling of Ti-6Al-4 V under hybrid nanofluids-assisted MQL conditions is investigated experimentally. The influence of $Al_2O_3$-MWCNTs on the milling force, temperature, and surface roughness is analyzed, respectively. The following conclusions are drawn:

1. In the milling of Ti-6Al-4 V, the flow rate was the most significant parameter that influenced resultant force, followed by concentration and flow rate. It could be associated with the tribo-film formation due to the high concentration of hybrid nanofluids (0.24 wt%), showing excellent lubrication, regarding load carrying and wear resistance at 160 mL/h.
2. Regarding the cutting temperature, hybrid nanofluids-assisted MQL reduced the shearing and frictional heat generation resulting in less cutting temperature. The MQL flow rate played a significant role in the reduction of cutting temperature, followed by concentration and air pressure. The hybrid nanofluids prevented direct contact of the cutting tool with the workpiece to limit the cutting heat generation.
3. In respect of surface roughness, a significant improvement in surface quality was observed due to a reduction in chip adhesion, severe BUE formations, and a smooth

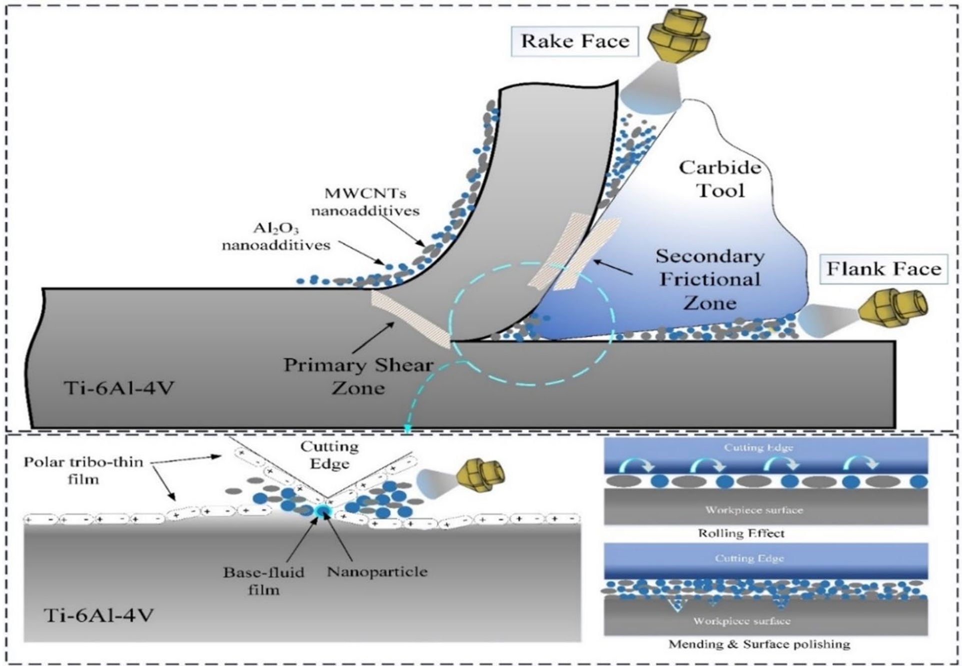


**Fig. 14** The hybrid nanofluids mechanism and effect on machining Ti-6Al-4 V

machine surface. A considerable reduction in surface roughness was noticed under the increase of nano-additives concentrations, followed by flow rate and air pressure. It can be associated with the different shapes of hybrid nanofluids behaving as ball-bearings and able to fill the micro-voids on the surface.

The SEM analysis of tool flank face depicted less severe tool edge damage, chip welding, and coating peeling under hybrid nanofluids. It principally can be attributed to the excellent penetration of nanofluids and formation of a protective layer on the tool surface to slide the chip. Also, chip analysis depicts the clean back surface and less melting of saw-tooth chip edges. The surface topography confirms the less micro-adhesion of chips and material debris.

**Author contribution** **Muhammad Jamil:** Conceptualization, data curation, formal analysis, methodology, writing—original draft, and writing—review and editing.

**Ning He**: Data curation, formal analysis, software, visualization, and writing—original draft.

**Wei Zhao**: Data curation, formal analysis, software, and writing—original draft.

**Aqib Mashood Khan**: Data curation, software, validation, and writing—original draft.

**Rashid Ali Laghari**: Conceptualization, project administration, validation, and writing—review and editing.

**Funding** The work is funded by the National Key Research and Development Project (2020YFB2010601).

**Availability of data and material** Not applicable.

**Code availability** Not applicable.

## Declarations

**Ethics approval** Not applicable.

**Consent to participate** Not applicable.

**Consent for publication** Not applicable.

**Competing interests** The authors declare no competing interests.

## References


1. Mia M, Gupta MK, Lozano JA et al (2019) Multi-objective optimization and life cycle assessment of eco-friendly cryogenic N2 assisted turning of Ti-6Al-4V. J Clean Prod 210:121–133. https://doi.org/10.1016/j.jclepro.2018.10.334
2. Paul S, Singh AK, Ghosh A (2017) Grinding of Ti-6Al-4V under small quantity cooling lubrication environment using alumina and MWCNT nanofluids. Mater Manuf Process. https://doi.org/10.1080/10426914.2016.1257797
3. Darshan C, Jain S, Dogra M et al (2019) Machinability improvement in Inconel-718 by enhanced tribological and thermal environment using textured tool. J Therm Anal Calorim. https://doi.org/10.1007/s10973-019-08121-y
4. Carvalho DOA, da Silva LRR, Sopchenski L et al (2019) Performance evaluation of vegetable-based cutting fluids in turning of AISI 1050 steel. Int J Adv Manuf Technol. https://doi.org/10.1007/s00170-019-03636-y
5. Khan AM, Jamil M, Ul Haq A et al (2018) Sustainable machining. Modeling and optimization of temperature and surface roughness in the milling of AISI D2 steel. Ind Lubr Tribol 71:267–277
6. Yıldırım ÇV, Kıvak T, Sarıkaya M, Erzincanlı F (2017) Determination of MQL parameters contributing to sustainable machining in the

milling of nickel-base superalloy Waspaloy. Arab J Sci Eng. https://doi.org/10.1007/s13369-017-2594-z
7. Ibrahim AMM, Li W, Xiao H et al (2020) Energy conservation and environmental sustainability during grinding operation of Ti–6Al–4V alloys via eco-friendly oil/graphene nano additive and minimum quantity lubrication. Tribol Int 150:106387. https://doi.org/10.1016/j.triboint.2020.106387
8. Günan F, Kıvak T, Yıldırım ÇV, Sarıkaya M (2020) Performance evaluation of MQL with AL2O3 mixed nanofluids prepared at different concentrations in milling of Hastelloy C276 alloy. J Market Res 9:10386–10400. https://doi.org/10.1016/j.jmrt.2020.07.018
9. Saidur R, Leong KY, Mohammad HA (2011) A review on applications and challenges of nanofluids. Renew Sustain Energy Rev. https://doi.org/10.1016/j.rser.2010.11.035
10. Sidik NAC, Samion S, Ghaderian J, Yazid MNAWM (2017) Recent progress on the application of nanofluids in minimum quantity lubrication machining: a review. Int J Heat Mass Transfer
11. Hegab H, Kishawy HA, Gadallah MH et al (2018) On machining of Ti-6Al-4V using multi-walled carbon nanotubes-based nano-fluid under minimum quantity lubrication. Int J Adv Manuf Technol 97:1593–1603. https://doi.org/10.1007/s00170-018-2028-4
12. Şirin Ş, Sarıkaya M, Yıldırım ÇV, Kıvak T (2021) Machinability performance of nickel alloy X-750 with SiAlON ceramic cutting tool under dry, MQL and hBN mixed nanofluid-MQL. Tribol Int 153:106673. https://doi.org/10.1016/j.triboint.2020.106673
13. Behera BC, Alemayehu H, Ghosh S, Rao PV (2017) A comparative study of recent lubri-coolant strategies for turning of Ni-based superalloy. J Manuf Process 30:541–552. https://doi.org/10.1016/j.jmapro.2017.10.027
14. Şirin E, Kıvak T, Yıldırım ÇV (2021) Effects of mono/hybrid nanofluid strategies and surfactants on machining performance in the drilling of Hastelloy X. Tribol Int 157:106894. https://doi.org/10.1016/j.triboint.2021.106894
15. Safiei W, Rahman MM, Yusoff AR et al (2021) Effects of SiO2-Al2O3-ZrO2 tri-hybrid nanofluids on surface roughness and cutting temperature in end milling process of aluminum alloy 6061–T6 using uncoated and coated cutting inserts with minimal quantity lubricant method. Arab J Sci Eng. https://doi.org/10.1007/s13369-021-05533-7
16. Ahammed N, Asirvatham LG, Wongwises S (2016) Entropy generation analysis of graphene–alumina hybrid nanofluid in multiport minichannel heat exchanger coupled with thermoelectric cooler. Int J Heat Mass Transf. https://doi.org/10.1016/j.ijheatmasstransfer.2016.07.070
17. Jamil M, Khan AM, Hegab H et al (2019) Effects of hybrid Al2O3-CNT nanofluids and cryogenic cooling on machining of Ti–6Al–4V. Int J Adv Manuf Technol 102:3895–3909. https://doi.org/10.1007/s00170-019-03485-9
18. Nine MJ, Batmunkh M, Kim JH et al (2012) Investigation of Al 2O 3-MWCNTs hybrid dispersion in water and their thermal characterization. J Nanosci Nanotechnol. https://doi.org/10.1166/jnn.2012.6193
19. Zhang Y, Li C, Jia D et al (2016) Experimental study on the effect of nanoparticle concentration on the lubricating property of nanofluids for MQL grinding of Ni-based alloy. J Mater Process Technol 232:100–115. https://doi.org/10.1016/j.jmatprotec.2016.01.031
20. Hegab H, Umer U, Deiab I, Kishawy H (2018) Performance evaluation of Ti–6Al–4V machining using nano-cutting fluids under minimum quantity lubrication. Int J Adv Manuf Technol 95:4229–4241. https://doi.org/10.1007/s00170-017-1527-z
21. Sharma AK, Katiyar JK, Bhaumik S, Roy S (2018) Influence of alumina/MWCNT hybrid nanoparticle additives on tribological properties of lubricants in turning operations. Friction. https://doi.org/10.1007/s40544-018-0199-5
22. Kumar Sharma A, Kumar Tiwari A, Rai Dixit A, Kumar Singh R (2019) Measurement of machining forces and surface roughness in turning of AISI 304 steel using alumina-MWCNT hybrid nanoparticles enriched cutting fluid. Measurement 107078. https://doi.org/10.1016/j.measurement.2019.107078
23. Mia M, Dhar NR (2017) Influence of single and dual cryogenic jets on machinability characteristics in turning of Ti-6Al-4V. Proc Inst Mech Eng B J Eng Manuf. https://doi.org/10.1177/0954405417737581
24. Heigel JC, Whitenton E, Lane B et al (2017) Infrared measurement of the temperature at the tool–chip interface while machining Ti–6Al–4V. J Mater Process Technol. https://doi.org/10.1016/j.jmatprotec.2016.11.026
25. Hadad MJ, Tawakoli T, Sadeghi MH, Sadeghi B (2012) Temperature and energy partition in minimum quantity lubrication-MQL grinding process. Int J Mach Tools Manuf. https://doi.org/10.1016/j.ijmachtools.2011.11.010
26. Li KM, Liang SY (2006) Modeling of cutting temperature in near dry machining. J Manuf Sci Eng Trans ASME. https://doi.org/10.1115/1.2162907
27. Gupta, M.K., Khan, A.M., Song, Q. et al (2021) A review on conventional and advanced minimum quantity lubrication approaches on performance measures of grinding process. Int J Adv Manuf Technol 117, 729–750. https://doi.org/10.1007/s00170-021-07785-x
28. Li B, Li C, Zhang Y et al (2017) Heat transfer performance of MQL grinding with different nanofluids for Ni-based alloys using vegetable oil. J Clean Prod. https://doi.org/10.1016/j.jclepro.2017.03.213
29. Alauddin M, El Baradie MA, Hashmi MSJ (1996) Modelling of cutting force in end milling Inconel 718. J Mater Process Technol. https://doi.org/10.1016/0924-0136(95)02113-2
30. Nam JS, Lee PH, Lee SW (2011) Experimental characterization of micro-drilling process using nanofluid minimum quantity lubrication. Int J Mach Tools Manuf. https://doi.org/10.1016/j.ijmachtools.2011.04.005
31. Said Z, Gupta M, Hegab H et al (2019) A comprehensive review on minimum quantity lubrication (MQL) in machining processes using nano-cutting fluids. Int J Adv Manuf Technol. https://doi.org/10.1007/s00170-019-04382-x
32. Gupta MK, Jamil M, Wang X et al (2019) Performance evaluation of vegetable oil-based nano-cutting fluids in environmentally friendly machining of Inconel-800 alloy. Materials 12:2792. https://doi.org/10.3390/ma12172792
33. Sharma AK, Tiwari AK, Dixit AR (2018) Prediction of temperature distribution over cutting tool with alumina-MWCNT hybrid nanofluid using computational fluid dynamics (CFD) analysis. Int J Adv Manuf Technol 97:427–439. https://doi.org/10.1007/s00170-018-1946-5
34. Jamil M, Khan AM, Hegab H et al (2020) Milling of Ti–6Al–4V under hybrid Al2O3-MWCNT nanofluids considering energy consumption, surface quality, and tool wear: a sustainable machining. Int J Adv Manuf Technol 107:4141–4157. https://doi.org/10.1007/s00170-020-05296-9
35. Ezugwu EO, Wang ZM (1997) Titanium alloys and their machinability - a review. J Mater Process Technol 68:262–274. https://doi.org/10.1016/S0924-0136(96)00030-1
36. Jamil M, Khan AM, Gupta MK et al (2020) Influence of CO2-snow and subzero MQL on thermal aspects in the machining of Ti-6Al-4V. Appl Therm Eng 177:115480. https://doi.org/10.1016/j.applthermaleng.2020.115480
37. Yıldırım ÇV (2019) Experimental comparison of the performance of nanofluids, cryogenic and hybrid cooling in turning of Inconel 625. Tribol Int. https://doi.org/10.1016/j.triboint.2019.05.014